Ultrasensitive On-Chip Immunoassays with a Nanoparticle-Assembled Photonic Crystal

Jin-Hee Han,[†] L. Sudheendra,[†] Hee-Joo Kim,[‡] Shirley J. Gee,[‡] Bruce D. Hammock,[‡] and Ian M. Kennedy[†,*]

Departments of [†]Mechanical and Aerospace Engineering and [‡]Entomology, University of California, Davis, California 95616, United States

ABSTRACT

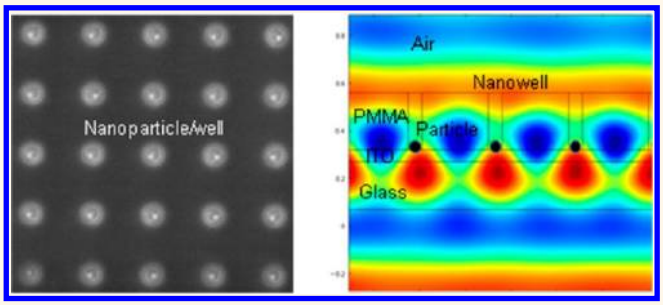

Electrophoretic particle entrapment system (EPES) is employed to generate 2D array of nanoparticles coated with biological molecules (*i.e.*, antibodies). Phase matching of the excitation and the emission in the 2D arrays with particles produces a highly enhanced fluorescence signal that was shown to improve the limit of detection in immunoassays. The phase matching is achieved when the particle are in the sub-100 nm range. A comparison between different size particles shows that the sensitivity of an immunoassay is extended to a range that is difficult to achieve with standard technology (*e.g.*, enzyme-linked immunosorbent assay-ELISA). The effectiveness of this novel configuration of particle-in-a-well was demonstrated with an assay for human epidermal growth factor receptor 2 (HER2; breast cancer biomarker), with a detection limit as low as 10 attomolar (aM) in less than 10 μL of serum-based sample. The limit of detection of HER2 indicated far superior assay performance compared to the corresponding standard 96-well plate-based ELISA. The particle-based photonic platform reduces the reagent volume and the time for performing an assay in comparison to competing methods. The simplicity of operation and the level of sensitivity demonstrated here can be used for rapid and early stage detection of biomarkers.

KEYWORDS: electrophoretic particle entrapment system (EPES) · nanoparticles · nanoarray · immunoassay · human epidermal growth factor receptor 2 (HER2)

Miniaturization continues to be a dominant theme in the development of new instrumentation for biological research. Although conventional microarrays have facilitated many breakthroughs in life sciences by identifying specific gene sequences or protein analytes,[1,2] further reduction in size to a nanoscale can offer significant advantages, particularly improvement in the assay speed.[3] However, the reduction in the size of an array poses problems that are related to a low signal-to-noise ratio and detectability of the signal. The detectable size of the spots in a microarray is limited by optical resolution to dimensions of approximately a visible wavelength. To overcome such a complication, many nanoarray-based detection schemes have relied on the development of high-resolution sensing (*i.e.*, atomic force microscope,[4] Kelvin probe force microscope,[5] and total internal reflection fluorescent microscope[6]).

Photonic crystals (PC) have been applied in a variety of ways for enhanced biosensing.[7−16] PCs have been assembled *via* colloids,[10−13] but this leads to complex structures that are not robust and ideal for disease diagnosis and proteomics. The sensing element in these cases was attached to the surface of a photonic crystal. These platforms provide a great improvement in the signal-to-noise ratio due to the photonic effects but rely on standard protocols to perform the immunoassay, thereby requiring copious amounts of antibodies and time-consuming washing steps. Such an approach does little to alleviate nonspecific binding issues. Here we show the advantage of a particle-based assay, in conjunction with the PC structure, to provide a new generation of supersensitive bioassay. Particles are commonly used as solid supports for antibody immobilization to improve the control of antibody concentration, to improve the speed of assays, and to facilitate separation from solution by making use of the well-controlled surface area, surface charge, functional groups, and choice of signal transduction that particles can provide.[17−22] For example, Haukanes and Kvam[17] demonstrated the effectiveness of using magnetic particles in bioassays for cell separation and isolation of specific nucleic acid sequence. Jager and Rijkers[22] compared the characteristics of a particle-based immunoassay to conventional ELISA for detection of cytokine. The particle-based multiplex

* Address correspondence to imkennedy@ucdavis.edu.

Received for review April 15, 2012 and accepted September 9, 2012.

Published online September 09, 2012
10.1021/nn301656c

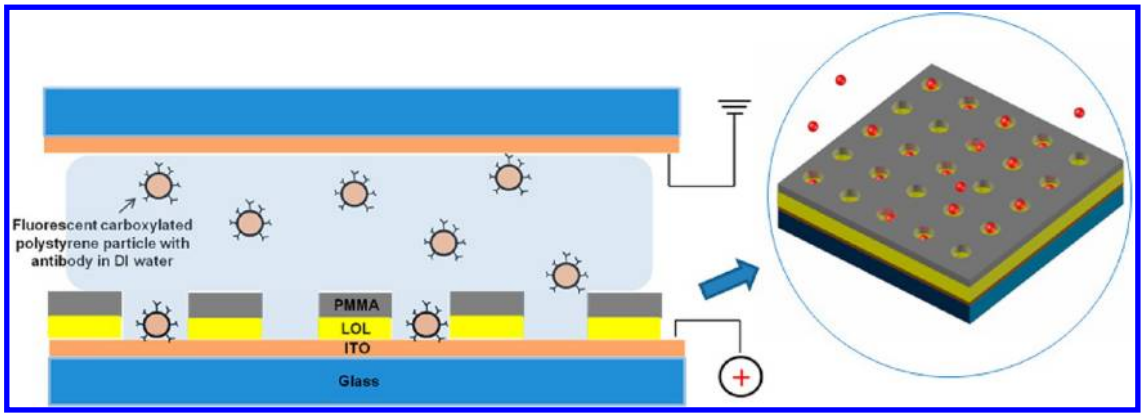

Figure 1. EPES and nanoarray. 2-D front view of the EPES; the ITO surface of the patterned PMMA-LOL-ITO glass slide (bottom) was connected to the positive terminal, while the ITO surface of the ITO glass slide (top) was connected to the ground terminal. The thickness of LOL 2000 nm and PMMA was 155 and 85 nm, respectively. The solution between the slides consisted of the negatively charged nanoparticles and deionized (DI) water; Inside circle shows a 3D view of the nanoarray with trapped particles.

immunoassay showed the superiority in terms of sensitivity, detection speed and minimization of the sample volume. The typical limit of detection (LOD) for the particle based multiplex immunoassay was a few pg/mL level and the assay time was hours. In addition, Becton Dickinson Biosciences (San Diego, CA)[18] have developed a particle-based cytometric array system using micrometer-sized particles and optical detection with extensive multiplexing capability and LOD at the pg/mL level for various human cytokines. As we shall show, the introduction of the nanoparticle into the photonic structure may confer an additional advantage in terms of detectability of fluorophore labels that are confined to the vicinity of the wells.

Our immunoplatform is simple, affordable, and provides an alternative method for the generation of functionalized arrays at the nanoscale. Our unique method of electrophoretic trapping of antibody-functionalized nanoparticles into nanowells of specific sizes has been demonstrated to yield a highly effective array that can be generated simply with a 2 V direct current (DC) source on an indium tin oxide (ITO)-coated glass slide.[23] Our results show that reducing the size of the particles is critical in realizing the advantages offered by the PC structure. The nanostructured PC-microarrays of nanoparticles-in-wells provide complete immuno-platforms with an assay completed on a single chip and with sensitivity that is vastly superior to conventional immunoassays with significantly shorter assay times and much smaller volumes of sample.

RESULTS

Electrophoretic Particle Entrapment in Nano- or Microwells. An electrophoretic particle entrapment system (EPES) was used to trap carboxylated polystyrene particles conjugated with capture antibodies into the PC structures engineered into a polymethyl methacrylate (PMMA)-lift off layer (LOL) 2000-ITO glass slide. The PC patterned chip was placed on a solid mantle with another ITO glass slide placed parallel on the top (Figure 1). The ITO at the bottom of the well was used as the electrode. The slides were each equipped with microscale manipulators to precisely control the location of the top and bottom slides horizontally or vertically. To create perpendicular electrophoretic forces, the bottom slide was connected to the positive electrical terminal while the top slide was connected to the ground terminal. The nanoparticles were added to the surface of the patterned bottom slide in a droplet of deionized water. The upper ITO glass slide was then placed onto the droplet. The distance between two slides was 490 μm. The surface charge of the suspended particles was negative due to the carboxyl terminal group on the particles. After placing the top ITO glass slide onto the droplet of particle solution and turning on the voltage, negatively charged particles migrated toward the surface of opposite electrical polarity. The EPES was operated for 15 min to 1 h. The operating time was adjusted to accommodate particles of different sizes considering zeta-potential measurements and the number of wells on the array. The number of wells on an array was 5476 wells with 40 nm particles, 625 wells with 200 nm particles, 25 wells with 1 μm particles, and one well with 5 μm particles. The applied voltage was 2 V (DC) during the EPES process. Each particle conjugated with the antibodies was trapped into the wells based on their diameter and the size of the well. The size of the wells for 40 nm, 200 nm, 1 μm, and 5 μm particles was 60 nm, 250 nm, 1.5 μm, and 7 μm, respectively. Multiple sizes of wells can be used, in principle, for which the largest particles are added to the chip first and occupy all the large wells, followed sequentially by decreasing particle size.

Particles were not found at the surface of the PMMA as seen in Figure 2a–d. In addition, only a single particle was trapped into its corresponding well (Figure 2e,f). After trapping, the solution between the two slides was removed by sliding the top ITO glass

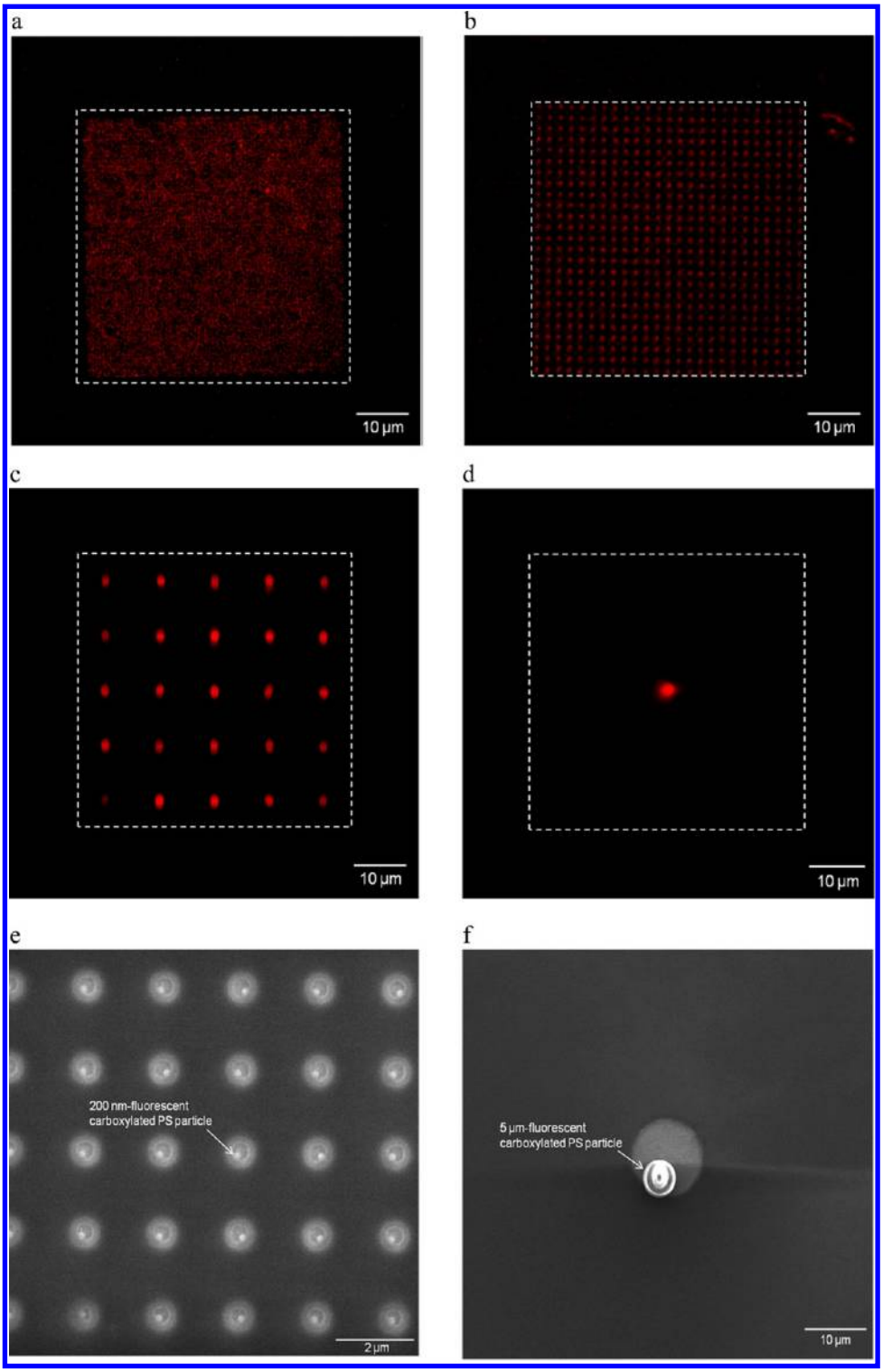

Figure 2. The nano- or microarrays/well with fluorescent carboxylated polystyrene particle (ex: 650 nm, em: 690 nm) conjugated with goat-anti-RIgG located to corresponding wells based on the size of particle after trapping using the EPES. (a) Fluorescent images of 40 nm particle/wells with 650 nm periodicity, (b) 200 nm particles/wells with 2 μm periodicity, (c) 1 μm particle/wells with 10 μm periodicity, (d) 5 μm particle/well, (e) scanning electron microscope (SEM) images of 200 nm particles/wells, (f) SEM images of 5 μm particle/well. White broken line indicates detection area (52 $\times$ 52 μm) where the excitation laser was focused and emitted fluorescent signal was collected.

slide parallel to the bottom slide with the voltage still on. The surface tension of the droplet liquid was sufficient to completely remove untrapped particles from the surface. There was no additional rinsing procedure for removing nonspecifically bound particles from the surface of the chip.

Optical Analysis. To understand the interaction of electromagnetic radiation with the arrays generated

with various sizes of particles, the fabricated PC structures with particles in the wells were modeled by employing the electromagnetic wave model in the RF module of COMSOL Multiphysics (v. 4.1; COMSOL Inc., Burlington, MA, U.S.A.). Normal incidence of the transverse electric (TE) field of the incoming electromagnetic wave was assumed, consistent with the experimental conditions. Maxwell's equations were solved for the given frequency, electric field of the TE mode of electromagnetic wave, and the refractive index and the geometry of the PC. Figure 3a shows the 3-D geometry of the nanostructured microarray with boundary conditions used in the model. The thickness of the PMMA/LOL and ITO was 240 and 50 nm, respectively. The width (*W*) of the well and its periodicity were varied based on the size of the particles. Width/periodicity (*D*) was 60 nm/650 nm for 40 nm particles, 250 nm/2 μm for 200 nm particles, and 1.5 μm/10 μm for 1 μm particles (modeling was not performed for the 5 μm well). The periodicity for different particles was chosen to provide uniformity of the particle distribution over the area of the array (52 $\times$ 52 μm). In a given area of the array, the periodicity was varied such that the ratio of periodicity and the particle diameter was $\sim$10. The particle distribution with corresponding periodicity also provided almost the same surface area coated with capture antibodies for each particle size case (for 40 nm-nanoarray, the surface area is 2.85 times less than that of 200 nm, 1 μm, and 5 μm array/well). Holding the surface areas approximately constant, and hence the total amount of antibodies available for binding approximately constant, allowed us to focus on the effects of the PC on signal enhancement and detection.

Supporting Information, Table S1 shows the material properties of polymethyl methacrylate (PMMA), glass, polystyrene, air, and indium tin oxide (ITO) used for modeling. The coating layer of the photoresists was assumed to be a single layer of PMMA because the difference of permittivity between the PMMA and the LOL was not significant. A scattering boundary condition was adopted in the model. Based on the measured power of the 532 nm laser diode intensity focused on the PC, the boundary value of the incoming electric field was set to 6140 V/m. The electric fields at the other boundaries were set to zero. The same boundary conditions were used in all cases. Figure 3b–g shows the spatial distribution of the electric field intensity confined within the PC. Frequencies of the electromagnetic (EM) wave corresponded to the excitation (maximum 532 nm) and emission (maximum 555 nm) spectra of the fluorophore: 5.64×10^{14} and 5.4×10^{14} Hz were used, respectively. For a 40 nm nanoarray with 650 nm periodicity, we observed the resonance in the PC structure for the wavelength between 532 and 555 nm.

To experimentally verify the presence of resonances due to the periodic nanostructure, two different refractive index materials, glycerin (refractive index: 1.47), and water (1.33) were added to the particle-based immunocomplex contained in the array of 40 nm wells. The intensity of the fluorescence was measured after the addition of each of the fluids and was compared to the intensity observed when air was the surrounding medium. For each test, rabbit-immunoglobulin G (RIgG) was used to construct the immunocomplex on the particles under the same conditions that were used for the main experiments. The addition of water to the top of the chip caused a 1.3$\times$ decrease in the measured fluorescence; the addition of glycerin caused a 6-fold reduction in fluorescence signal (Supporting Information, Table S2). The reduction of signal with reduction in relative difference in refractive index is consistent with the suppression of PC behavior, which is refractive index dependent.

To understand the effect of the particle in the PC structure, a numerical model with 40 nm particles with 650 nm periodicity was compared with the 200 nm particles with the same periodicity. For the wavelengths of interest (532–555 nm), the results showed that the size of the nanoparticle is an important parameter in achieving resonance (Supporting Information, Figure S1). For particles in excess of 100 nm, the size of the particle also imposed restrictions on the periodicity and the depth of the well. These are important parameters that determine the phase matching of the waves due to the periodic structure, such a grating.[24] For example, the depth of the periodic structure, ℓ, must satisfy the relation $\lambda_G/2 > \ell > \lambda_G/4$ for first order diffraction, where λ_G is the wavelength of the light experiencing the guided mode resonances. Therefore, considering the emission wavelength of Alexa-532, the effective range of the depth is 278 nm $> \ell >$ 139 nm. The numerical model of these particles in a periodic array shows that the incorporation of 40 nm particles into the wells efficiently utilizes the tail of the evanescent field that extends into the superstrate region (PMMA) for excitation of the fluorophores on its surface. Larger particles such as the 1 μm particles that were incorporated into an array showed strong Mie scattering due to the large diameter of the particle.[25] The Mie scattering interferes with the Bragg scattering and inhibits the phase matching required for fluorescence enhancement.

Detection of Rabbit-Immunoglobulin G (RIgG): Comparison between Nanostructured and Microstructured Arrays. Immunoassay experiments were performed to prove for the limit of detection for nano and microstructured arrays. A single-photon counting detection system was used along with a 532 nm laser for excitation. Light at a wavelength of 555 nm emitted was collected from the immunocomplex on the detection area of the array (52 $\times$ 52 μm; white broken line in Figure 2a–d). Figure 4 shows the standard curves for four different arrays based on the size of particles (40 nm, 200 nm,

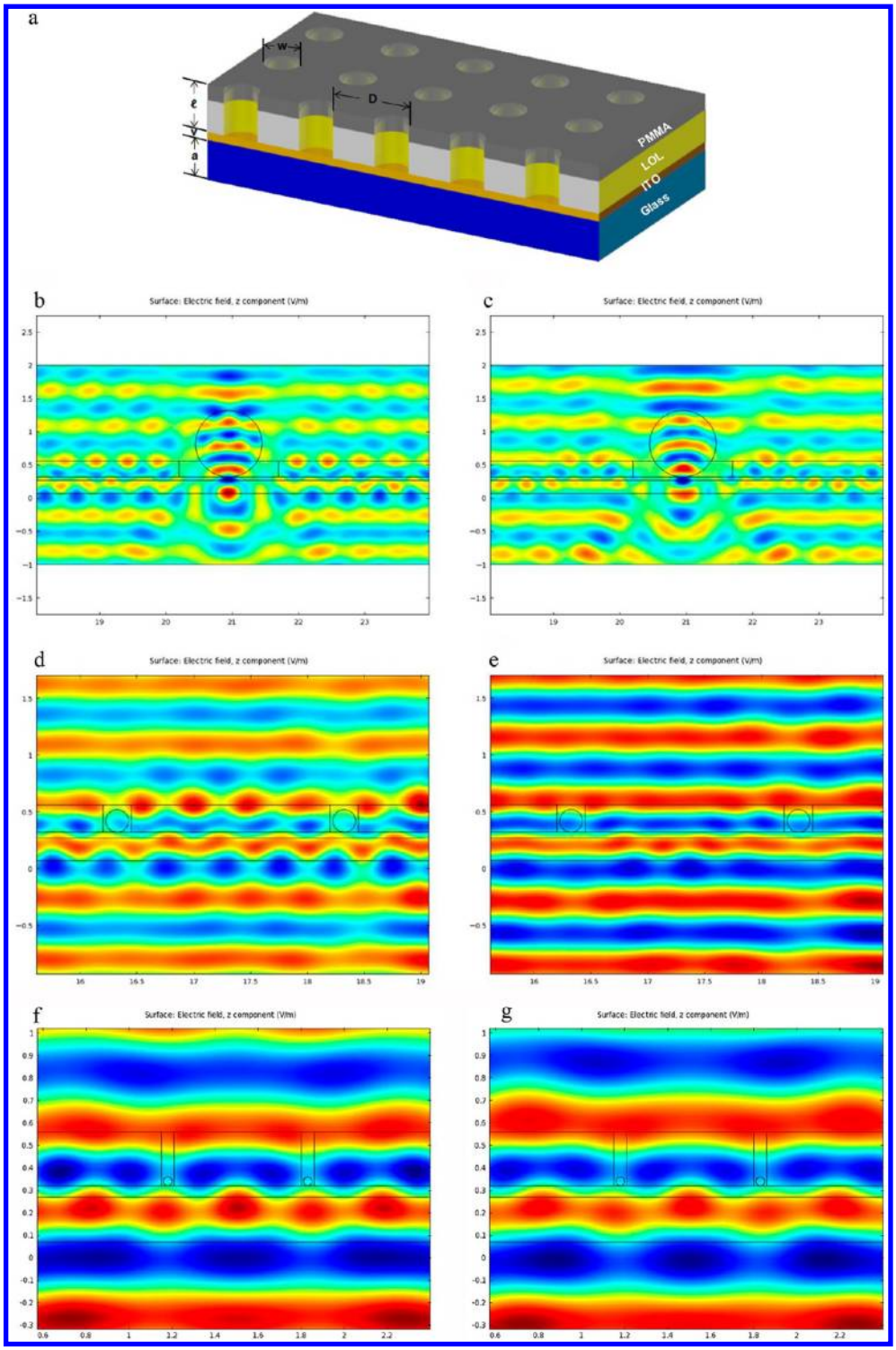

Figure 3. Numerical modeling of the nanoarray with PC structure. (a) 3-D geometry of the nanoarray; *W*/*D*: 60 nm/650 nm (40 nm particle), 250 nm/2 μm (200 nm particle), 1.5 μm/10 μm (1 μm particle), 7 μm/0 μm (5 μm particle); *v*: 50 nm; *l*: 240 nm (85 nm PMMA and 155 nm LOL; PMMA and LOL 2000 were assumed to be single layer in the model), *a*: 1.1 mm, (b) spatial distribution of the electric field intensity confined within 1 μm PC-microarray for 532 nm wavelength, (c) 1 μm PC-microarray for 555 nm wavelength, (d) 200 nm PC-nanoarray for 532 nm, (e) 200 nm PC-nanoarray for 555 nm, (f) 40 nm PC-nanoarray with 650 nm eriodicity for 532 nm, (g) 40 nm PC-nanoarray with 650 nm periodicity for 555 nm.

1 μm, and 5 μm). Nine different concentrations of RIgG dissolved in phosphate buffered saline (PBS) were detected using sandwich immunoassays: 10^{-3}, 1, 10^3, 10^4, 10^5, 10^6, 10^7, 10^8, and 10^9 pg/mL. A goat-anti-RIgG−Alexa 532 conjugate was used as a fluorescently labeled detection antibody at a concentration of 10^7 pg/mL. Background noise that originated from the 532 nm laser was measured by shining the

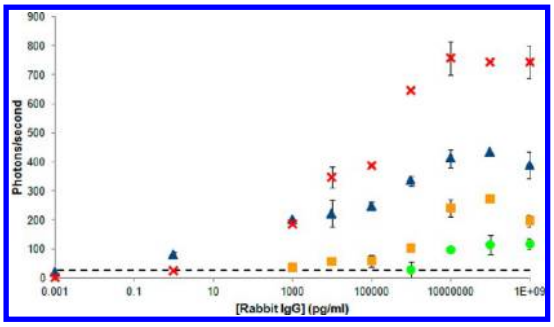

Figure 4. Detection of RIgG on the nano- or microarrays/well (40 nm, 200 nm, 1 μm, and 5 μm) with single photon counting detection system: ×, 40 nm nanoarray; ▲, 200 nm nanoarray; ■, 1 μm microarray; ●, 5 μm microwell. Nine different concentrations of RIgG dissolved in PBS buffer were used: 10^{-3}, 1, 10^3, 10^4, 10^5, 10^6, 10^7, 10^8, and 10^9 pg/mL. The photons of light emitted from the immunocomplex were then detected by the single photon counting avalanche photodiode, which generated a pulse per a photon. The pulses generated for a second were counted. One datum point on the curve was obtained from averaged value of pulses per second for 20 s using the oscilloscope. LODs were determined from the signal (dash lines) equal to the background noise with three times standard deviation of the background noise. Error bars, standard deviation over three replicates.

laser on the arrays in the absence of particles and immunoassay reagents. The measured background photon count rate was 13 ± 4 photons/second. To test for nonspecific binding of the fluorescent-labeled detection antibody to either the particle-goat-anti-RIgG or the surface of the PMMA, the solution of the detection antibody was added to the arrays that were comprised of trapped particles conjugated with goat-anti-RIgG without the target. The signal generated by nonspecific binding of the detection antibody averaged 26 photons/second (background noise included) for wells of all sizes, with no statistically significant differences compared to the background noise ($p < 0.05$). Additionally, a negative control for goat-anti-RIgG (capture and detection antibody) with another target (10^7 pg/mL of mouse IgG) averaged 19 photons/second (background noise included) for all size cases, showing that negligible background signals were observed when the mouse IgG was used as a target molecule due to negligible cross reactivity of the goat-anti-RIgG to the mouse IgG. The data points on the standard curve were corrected by subtracting nonspecific binding (background noise excluded) from total signals (Supporting Information, Table S3).

The 40 nm nanoarray with 650 nm periodicity showed the highest intensity of fluorescent signal from the array and the most sensitive detection of analyte (slope of the curve). The intensity decreased as the size of the particles/wells increased. The 40 and 200 nm particles (well periodicity of 2 μm) showed the best limits of detection (LOD) at 1 pg/mL, corresponding to 7 femtomolar concentration of the RIgG (molecular weight: 144 kDa), while the 1 μm particles (10 μm periodicity) and 5 μm particles yielded LODs of 10^3 and 10^6 pg/mL, respectively. The linear detection range was $1-10^7$ pg/mL (R^2: 0.92 or 0.94) for 40 and 200 nm particles, while it was 10^5 to 10^7 pg/mL (R^2: 0.91) and 10^6 to 10^7 pg/mL (nonestimated R^2 value based on only two datum points in the linear range) for 1 and 5 μm particles, respectively, indicating that the arrays pixelated with the nanoparticles showed a significantly greater linear detection range than a single microparticle in a particle based immunoassay. A nonoptimized nanostructure with 40 nm-particles (Figure 3f,g) exhibits a diffused electric field that does little to promote fluorescence emission. An enhanced electric field around the well should be able to increase the rate of fluorescence and thereby improve the limit of detection and the sensitivity toward an analyte. To achieve enhanced fluorescence, phase matching of the electromagnetic radiation with the periodic photonic structure, leading to a stronger, localized electric field, was found to be necessary.

Optimization of Fluorescence. Optimization of the PC structure was performed for the 40 nm nanoarray by applying the phase-matching formula to the electromagnetic radiation interacting with the PC structure.[24,26]

$$\sin(\theta) = (\beta \pm m2\pi/D)/n_1 k \quad (1)$$

where θ is the angle of incidence of light with respect to the normal to the PC structure surface. β is the in-plane propagation constant given by $\beta = n_2 k \cos(\varphi)$, m is the order of diffraction, D is the periodicity of the photonic structure, k is the wave vector given by $k = 2\pi/\lambda$, n_1 is the refractive index of the medium the light is incident, and n_2 is the refractive index of the photonic structure. Equation 1 applies in the limit of $\varphi \rightarrow 0°$, where φ is the internal diffraction angle between the diffracted light and surface; this approximation serves to provide a rough guide to designing the nanostructure. Solving for $\theta \rightarrow 0$ (for normal incidence),

$$D = \lambda m/n_2 \cdot \cos(\varphi) \quad (2)$$

Taking an average refractive index for the photonic structure to be $n_2 = 1.6$, for the first order of the diffraction and taking the wavelength for excitation and emission to be 532 and 555 nm, respectively, we obtain a value for D of ~350 nm for first order of diffraction. A numerical model based on this structure confirmed the formation of modes within this periodic structure (Figure 5a,b). Figure 5c showed the experimental standard curve for a RIgG immunoassay using an optimized array of 40 nm wells with 350 nm periodicity. This array of wells was compared experimentally with an array of 40 nm wells spaced with a 650 nm periodicity so that the total surface area covered with capture antibodies was about the same. The LOD in the optimized array was 10^{-3} pg/mL, corresponding to a 7 attomolar concentration of the RIgG, 1000-fold lower than of the LOD in a 40 nm nanoarray with the nonoptimal 650 nm periodicity. Two distinct log−linear detection ranges with different

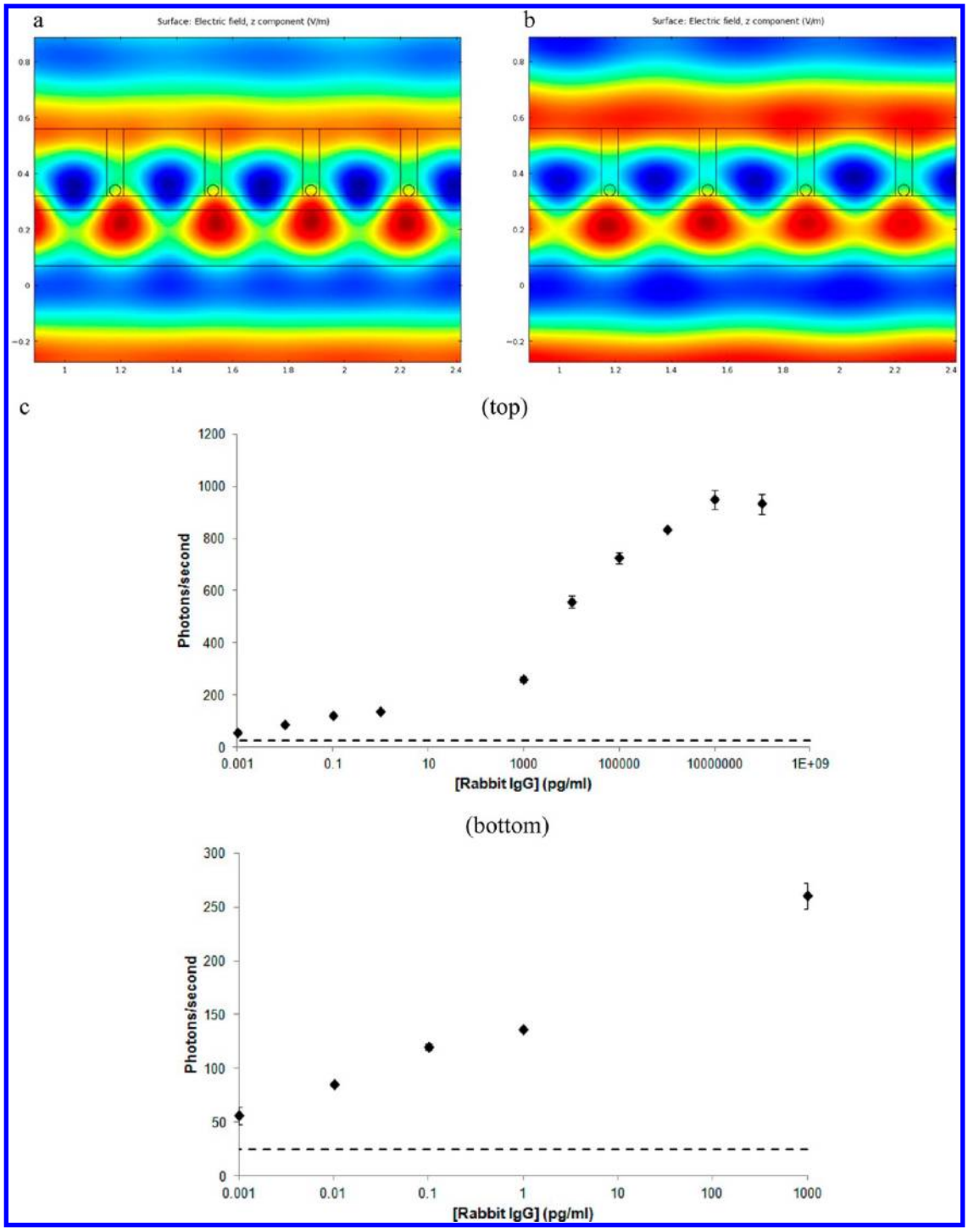

Figure 5. Optimization of PC structure of the nanoarray and immunoassay. (a) Spatial distribution of electric field in 40 nm nanoarray with 350 nm periodicity using the numerical model; 532 nm wavelength and (b) 555 nm wavelength. (c) The standard curve from the immunoassay of detecting RIgG using 40 nm nanoarray with 350 nm periodicity. The plot on top shows the assay response over the concentration range (10^{-3}–10^{8} pg/mL). The plot on bottom shows a quasi-linear response in the attomolar to picomolar range. Dash line is equal to the background noise with three times standard deviation of the background noise. Error bars, standard deviation over three replicates.

slopes were found at high concentrations (10^{3}–10^{7} pg/mL; R^2: 0.95) and at low concentrations (10^{-3}–10^{3} pg/mL; R^2: 0.99). The signal enhancement also depended on the choice of fluorophore used for the probe. Alexa 532 fluorophore showed the best spectral fit to take advantage of the PC structure in the optimized array because the peak wavelengths for both excitation and emission of the fluorophore was closely associated with enhanced electric fields observed in the numerical model (Supporting Information, Figure S2).

Detection of HER2 in Serum. Enhanced limits of detection can be of great benefit for the early diagnosis of

disease and infection. An immunoassay for HER2 positive breast cancer in human serum provides a convenient model for testing the practical value of the PC/nanoparticle assay given the ready availability of both antibodies and target molecules in known concentrations. In practice, however, the natural background levels of HER2 may obviate the need for the reduction of the LOD to very low levels. Figure 6 shows the standard curve for the HER2 immunoassay using the optimized array of 40 nm particles. In addition, a standard curve was obtained for the corresponding standard 96-well plate-based ELISA (five different concentrations of HER2 dissolved in PBS were used: 25.6, 128, 640, 32×10^2, and 16×10^3 pg/mL). The recombinant HER2 was spiked to 25% human serum to show the reliability in a clinical diagnosis. The mixing ratio of serum to PBS buffer was chosen to reduce matrix effects.[27] The concentration range was 10^{-3} to 10^7 pg/mL. Background noise was 13 ± 4 photons/second. Nonspecific binding of fluorescently labeled detection antibody to either the particle-monoclonal capture antibody to HER2 or to the surface of PMMA gave rise to a signal of 12 ± 2 photons/second (background noise excluded). To test for any false-positive effect caused by the residue of either unbound HER2 to the particle-capture antibody or fluorescently labeled detection antibody in the wells after incubation followed by removal of solution, the particles without capture antibody were used for an immunoassay on the array (other conditions were same). The signal was not different from the background noise. For a negative control, nonspiked serum in PBS was used; serum contains a number of different kinds of proteins with millimolar concentrations[28] that could present interferences in the assay. The signal difference between the negative control and background noise was negligible at one photon/second. The test results for nonspecific binding and the negative control were in the range of the background noise within three standard deviations.

The two distinct log−linear detection ranges for HER2 were found at 10^3−10^7 pg/mL (R^2: 0.99) and at 10^{-3}−10^3 pg/mL (R^2: 0.99). The limit of detection was 10^{-3} pg/mL, corresponding to a 10 attomolar concentration based on the molecular weight of recombinant HER2 (98.6 kDa, R&D systems). The LOD was 10^6-fold lower than that of standard 96-well plate-based ELISA measuring absorbance (1 ng/mL).

DISCUSSION

Our results have demonstrated the controlled delivery of biological reagents bound to particles to specific spots on a substrate through EPES. This controlled nanostructured is shown to yield significant improvements in the limit of detection for a variety of immunoassays for reasons that are discussed below.

To achieve a reproducible immunoassay, it is important to have reliable and consistent deposition of

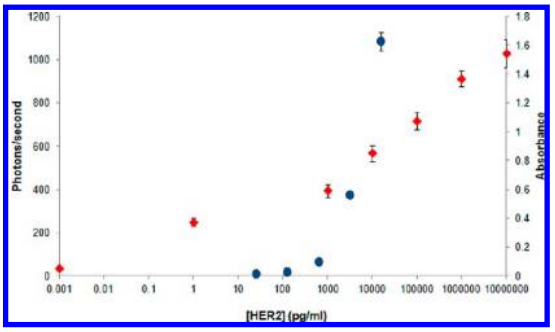

Figure 6. Detection of HER2 using 40 nm nanoarray with 350 nm periodicity (◆). The standard curve obtained from conventional 96-well plate-based ELISA was compared (●). Seven different concentrations of HER2 spiked into 25% human serum were used: 10^{-3}, 1, 10^3, 10^4, 10^5, 10^6, and 10^7 pg/mL on the nanoarray. In the case of conventional ELISA, five different concentrations of HER2 dissolved in PBS were used: 25.6, 128, 640, 32×10^2, and 16×10^3 pg/mL. Error bars, standard deviation over three replicates.

particles conjugated with biological molecules into their corresponding nanowells: the EPES method demonstrated 100% trapping efficiency given sufficient time (Figure 2a−f). By using a weak trapping force, the EPES easily resolved the problem of locating antibodies at multiple desired sites of the array in a short time without damage to the proteins. The size and location of the nanowells can be easily controlled leading to the possibility of high-throughput assays. Furthermore, EPES proved to be a simple yet effective way of removing either particle or biological molecules from the surface of the array by using the Couette-flow.

For the reliable application of our particle based PC/EPES system to the immunoassay, we used 40 nm particles-capture antibody in a pixelated nanoarray with PC structure for detecting breast cancer biomarker HER2 in serum. The LOD was improved a million-fold (10 aM) over the corresponding standard 96-well plate-based ELISA. As noted already, the detection limit in our assay is much better than is needed for clinical application of the HER2 assay because the threshold level to determine the existence of a breast cancer tumor is 15 ng/mL.[29] However, this model assay serves to demonstrate the significant advantages of using a particle-based immunocomplex within a PC structure that is constructed with nanoparticles in wells.

We exploited the advantages of particle-based assays by using the particles to construct a well-ordered nanoscale array of particles in a fast, efficient manner. Negative charges on the carboxylated particles enabled use of electrophoretic transport for localizing particles to nanoscale wells with an electrically conductive substrate (ITO) with positive charge at the bottom of each well. The PC structure is formed by a solid-bound immunocomplex, consisting of capture antibodies, analytes, and detection antibodies plus fluorophores, that sits on a high refractive index substrate (ITO). In a related concept, Ganesh *et al.*[30] explored leaky modes in nanostructures to enhance

emission from quantum dots dispersed on the PC surface. More recently, the same group has demonstrated up to 89% enhancement in the limits of detection of cancer biomarkers with a Cy5 dye and photonic structure.[8] Based on the available literature on phase-matched nanostructures with PC features and our experimental and modeling results, it is likely that guided mode resonances and mode coupling leading to leaky mode extraction play an important role in our fluorescence enhancement.

The combination of nanoparticles in an array of nanowells, constituting in effect a pixelated single microspot, is the key to achieving extremely low LOD. Pixelation of a microspot down to 40 nm with specific periodicity is the most important factor in coupling the Bragg scattering with resonances in a PC structure for signal extraction. For 200 nm particles in the PC structure, in the absence of resonance, diffraction still provides an enhancement of fluorescence.[31] The effects of diffraction vanish progressively with an increase in the size of the particles, leading to the observed deterioration in the LOD (Figure 4). The effect is most pronounced for the optimal combination of the smallest nanoparticles and nanowells with the correct spacing for first order diffraction. The size and spacing of the nanowells is dictated by the wavelengths of visible light that are used for excitation and emission. By comparing the LOD and log−linear detection range for 40 nm particles in a pixelated array with a single 5 μm particle in a well, we found that the use of the single photon counting detection system was not, by itself, the most important factor in obtaining femtomolar and attomolar level sensitivity. In fact, the sensitivity in a 40 nm particle pixelated nanoarray could be enhanced more that 1000-fold by optimizing just the PC structure.

In the detection of cancer biomarkers in serum, careful rinsing procedures are needed in general to reduce false-positive effects that arise from other proteins in the serum. Our method needed a simple one-time rinsing with a 10 μm droplet of deionized water for highly effective particle removal during the EPES process. The effectiveness of the simple rinsing procedure could be verified by demonstrating negligible values of the negative control compared to background noise using only serum. Nonspecific binding of carboxylated polystyrene particles to the PMMA surface was prevented due to the hydrophilic surface provided by carboxyl groups.[32] The spreading of a molecule on a surface is time-dependent:[33] our 20 min incubation time is shorter than the typical time (over 1 h) that is used for immobilizing antibodies on PMMA surface.[34,35] The short incubation time leads to less binding of proteins on a surface so that the Couette-flow that is established between the moving top plate and stationary bottom plate during the EPES washing procedure can easily remove proteins on the bare PMMA surface.

The remarkably low LOD is well beyond the limit indicated by the equilibrium dissociation constant, K_d. It should be recalled that femtomolar and subfemtomolar analyte concentrations are routinely detected by microarrays;[36] these levels are well below the levels associated with K_d. In a thorough analysis of immunoassay performance, Ekins *et al.*[37] estimated the minimum analyte population that is identifiable on a microspot; factors that can improve the LOD include an increased density of capture antibodies and relatively low concentrations of secondary detection antibodies. Chang *et al.*[38] described a novel array that worked on a digital basis by counting enzyme-linked immunocomplexes in a femtoliter well. They achieve single molecule detection, albeit at the expense of a somewhat more complex assay than the one that we are reporting. Citing skepticism with regard to their detection limits that are much lower than K_d, they undertook a thorough analysis of the system and arrived at the same conclusions as we and Ekin *et al.* did: under the right conditions, K_d does not impose a fundamental limit on the detection limit.

In the PC format, several factors combine to reduce the LOD to very low levels. It is known that the number of antibodies immobilized on particles can exceed the estimates based on the surface area of the particles.[39,40] Hence, we benefit from an increase in antibody density by using the nanoparticle to immobilize capture antibodies. In addition, our improvement in signal-to-noise ratio (a 10-fold improvement with 40 nm particles in comparison to a single 5 μm particle) leads to further enhancement in the LOD. Our simple analysis shows that K_d is not the controlling factor under a set of limiting conditions that we are able to satisfy. If the total antigen concentration [Ag] $\ll$ [Ab], where [Ab] is the total available capture antibody concentration, then [Ab] is approximately constant. Furthermore, if [Ab] $\gg K_d$, then it is straightforward to show that the concentration of the bound complex [AgAb] is approximately independent of K_d and proportional to [Ag] without considering the details of adsorption. These conditions are satisfied with our assay system and are only feasible as a result of the ultrasensitive detectability of the nanophotonic array, the density of capture antibodies, and the small scale of the microspot.

The very low detection limits that we report raise several interesting issues. Sheehan and Whitman[41] showed that the reduction of the size of a sensor to the nanoscale may not be advantageous in terms of the detection limits due to mass transport limitations. In other words, in a realistic assay time scale, very few analyte molecules will be able to diffuse to the sensor region from the sample volume, unless they are somehow directed. In our case, that may seem to contradict our results. However, it must be realized that our nanoparticles are distributed over a wide region in

arrays of 52 × 52 μm with a pitch of 650 nm or 26 × 26 μm with a pitch of 350 nm, so we are not limited by diffusion of analyte to a single nanospot; our sensor is effectively a distributed nanoarray and will exhibit mass transport limits that are more akin to a microarray.

Based on the concentration of the analyte in our 10 μL sample that covered 9 separate arrays, each 26 × 26 μm, we obtained an estimate of the likely number of analyte molecules that were captured, about five per individual array. With higher sensitivity in the assay, that is, greater slope of the standard curve at the low range, we might expect to see some quantization of the signal. However, our relative insensitivity to analyte concentration precluded the possibility of discerning single molecule binding events. The log−linear nature of the curve at low concentrations is suggestive of a Temkin isotherm for which there is a random distribution of binding energies at a surface. Johnson and Arnold[42] found that a Temkin isotherm offered a good fit to their measurements of protein adsorption to metal ligands on a surface for which there was a distribution of binding energies. Our primary capture antibodies were passively adsorbed onto the particles and therefore a random distribution of affinities and binding energies for analytes should be expected. For that case, and at very low concentrations, a Temkin isotherm presents a plausible model of the adsorption process under our experimental conditions. It is consistent with the log dependence on analyte concentration that we have seen in all of the assays that we considered. Greater sensitivity would be achieved with a covalent attachment of the antibodies to the particle surface but at the expense of available surface charge for the EPES process; we have found that EPES does not work following covalent attachment of antibodies. Magnetophoresis with superparamagnetic nanoparticles would be necessary in this case and is the subject of ongoing research.

Other studies have demonstrated femto- or attomolar sensitivity for immunoassays: a carbon nanotube based immunoassay with electrical transistor measurements detected environmental pollutants with a limit of detection (LOD) of 500 fM;[43] a DNA bar code method using magnetic particles for detecting prostate-specific antigen (PSA) demonstrated an LOD of 30 aM;[44] an electrochemical immunosensor using a gold-film-coated electrode and magnetic particles for detecting cancer biomarkers also yielded an LOD of 30 aM;[45] and a microarray-based immunoassay for detecting cytokines also showed a low-to-middle femtomolar sensitivity.[36] However, such methods still require complex, time-consuming efforts in fabrication of the device, sample preparation, and immobilization of biological molecules using self-assembled monolayer (SAM); these methods may also require interrogation of large sample volumes over a considerable amount of time. These disadvantages do not pertain to our PCEPES system. In comparison to those immunoassay techniques,[36,43−45] our PC-nanowell array/EPES is relatively simple to implement and requires less incubation time and a smaller volume of bioreagents for similar or better sensitivity than comparable subfemtomolar systems. This superiority translates to a rapid and field-deployable biosensor system that can be employed broadly for identifying biomarkers of disease or for illicit drug testing, among other potential applications.

CONCLUSION

We have reported a novel, yet simple, PC-immunoassay platform that is readily constructed by using nanoparticles that are conjugated with biological reagents. A facile electrophoretic particle trapping method was used to assemble a photonic crystal that enhances fluorescent signals while achieving extremely low background noise. In contrast to micrometer-sized particles that have been used in the past, sub-100 nm particles in nanowells fully exploit the enhanced fluorescence excitation and extraction that is afforded by coupling to the nanophotonic crystal structure with optimized periodicity. This enhancement translated to ultrasensitive detection of IgG and breast cancer biomarker at low attomolar concentrations, overcoming the limits imposed by antibody affinity in conventional immunoassays. The sensitivity and the speed of the assay performed on the PC-nanoarray demonstrated a ground-breaking concept in ultrasensitive bioassays that may provide new point-of-care tools for human health diagnostics and care.

METHODS

Materials. The 40 nm fluorescent carboxylated polystyrene (PS) nanoparticles (F-8789; ex: 660 nm/em: 680 nm) were purchased from Invitrogen (Carlsbad, CA). The 200 nm fluorescent carboxylated PS nanoparticles (FC02F/9770; 660/690) and 1 μm fluorescent carboxylated PS microparticles (FC04F/8608; 660/690) were purchased from Bangs Laboratories (Fishers, IN). The 5 μm fluorescent carboxylated PS microparticles (2308; ex: 660/685) were purchased from Phosphorex (Fall River, MA).

Goat-anti-RIgG and goat-anti-RIgG−Alexa 532 used for capture antibody and detection antibody, respectively, were purchased from Invitrogen. Monoclonal capture antibody to HER2 (MAB1129), biotinylated polyclonal detection antibody to HER2 (BAF1129), and recombinant HER2 were purchased from R&D Systems, Inc. (Minneapolis, MN). Streptavidin-Alexa 532 was purchased from Invitrogen. TMB (3,3′,5,5′-tetramethylbenzidine) was purchased from Sigma-Aldrich (St. Louis, MO). Streptavidin-horseradish peroxidase (HRP) was purchased from Pierce Thermo Pierce Scientific (Rockford, IL).

Indium tin oxide (ITO)-coated glass wafer (CG-81N-1515; resistance: 30−60 Ω) was purchased from Delta Technologies (Stillwater, MN). All chemicals used for fabrication of the arrays/well were obtained from the University of California—Davis, Northern California Nanotechnology Center: acetone (Sigma-Aldrich, St. Louis,

MO), LOL-2000 (MicroChem, Newton, MA), 2% 950 PMMA A2 (MicroChem), methyl isobutyl ketone (MIBK, Sigma-Aldrich), isopropyl alcohol (IPA, Mallinckrodt Baker), and CD-26 (tetramethylammonium hydroxide, MicroChem). A 100× infinity corrected objective lens (M Plan APO; NA: 0.7; working distance: 6.0 mm; focal length: 2 mm) was purchased from Mitutoyo (Kawasaki, Japan). The beam splitter (FF545/650-Di01), 532 nm long pass filter (BLP01-532R-25), 532 nm notch filter (NF01-532U-25), and 633 nm notch filter (NF02-633S-25) were purchased from Semrock (Rochester, NY). The single-photon counting avalanche photodiode (SPAD; SPCM-AQRH-13; dark count: 500 counts/s max) was purchased from PerkinElmer (Waltham, MA). The CCD camera (TCA-5.0C; 5.0 MP) for imaging the arrays/well with fluorescent particles was purchased from Tucsen Image Technology Inc. (FuJian, China).

Immunoassays on Nano/Microarrays/well. A 1 mL aliquot of 0.05% (w/v) fluorescent carboxylated polystyrene particles (40 nm, 200 nm, 1 μm, and 5 μm) were coated with goat-anti-RIgG by passive adsorption considering 100% bound coverage of the antibody to surface of the particle based on particle size. The amount of the antibody for full coverage was estimated by using a protocol provided by the vendor. To ensure a well-distributed monolayer of absorbed antibody, we used the antibody at a concentration three times greater than the concentration indicated by the data from the particle vendor (Bangs Laboratories, TechNote 205). The mixing time was 2 h at room temperature followed by overnight incubation at 4 °C. The mixed solution was then washed and finally suspended in DI water. After trapping the particle-goat-anti-RIgG into nano- or microwells corresponding to their sizes, 10 μL of target RIgG dissolved in 1× PBS buffer was dropped to the area where a total of nine arrays/well (the distance between the arrays/wells was 250 μm) were located, hence, the amounts of the target molecules in 10 μL were shared by an individual array that was the unit for signal harvesting. The arrays/wells were then incubated for 20 min at room temperature followed by removal of the solution. The solution is removed by the Couette-flow established between the moving top plate and the stationary bottom plate. Finally, 10 μL of 10^7 pg/mL goat-anti-RIgG−Alexa 532 dissolved in 1× PBS buffer was dropped onto the arrays/well. The chip was then incubated for another 20 min followed by removal of the solution. Concentrations of the target were varied from 10^{-3} to 10^9 pg/mL, while the concentration of fluorescently labeled antibody was fixed.

In addition, to demonstrate practical performance of the nanoparticle based PC-array in clinical diagnosis, HER2 was used as target. Monoclonal capture antibody to HER2 was coated onto 40 nm fluorescent carboxylated PS particles by using the same protocol used in case of goat-anti-RIgG. Biotinylated polyclonal detection antibody to HER2 was conjugated with streptavidin-Alexa 532 using a standard protocol. The volume of recombinant HER2 (target) and detection antibody-Alexa 532 used for each droplet onto the nanoarray was 10 μL. Detection antibody-Alexa 532 was used at fixed concentration of 10^7 pg/mL. The recombinant HER2 for the concentration range of 10^{-3}−10^7 pg/mL was spiked into 25% human serum. For the serum sample, to remove the proteins from the surface of the array, an additional rinsing procedure with 10 μL DI water was performed. The method for removal of the DI water was the same as that of the bioreagents. The data points on the standard curve from all immunoassays were obtained from three random replicates out of the nine arrays.

Conventional 96-Well Plate-Based ELISA for Detecting HER2. A 96-well ELISA plate (Maxisorp, Nunc) was coated with monoclonal capture antibody to HER2 at 8×10^6 pg/mL in PBS by 2 h incubation at 37 °C. Nonspecific sites of the plate were blocked with 400 μL of 1% BSA in PBS per each well, followed by 2 h incubation at 37 °C. A total of 100 μL of various concentrations of HER2 diluted in PBS (25.6, 128, 640, 32×10^2, 16×10^3 pg/mL) were added to wells and the plate was incubated for 1 h at room temperature with gentle rocking. The plate was washed five times with PBST and 100 μL of a biotinylated polyclonal detection antibody to HER2 was added. After a 1 h incubation at room temperature, the plate was washed five times with PBST, and then 100 μL of streptavidin-HRP (1/6000 dilution in PBS) was added and the plate was incubated at room temperature for 1 h. The plate was washed five times with PBST and 100 μL of the HRP substrate solution (400 μL of 0.6% TMB in DMSO and 100 μL of 1% H_2O_2 solution into 25 mL of citrate buffer) was added and the reaction was stopped after 15 min by adding 50 μL of 2 M H_2SO_4 solution. Absorbance was obtained by reading the plate at 450 nm with a plate reader (Molecular Device, Sunnyvale, CA).

Photonic Nano/Microarrays/Well Fabrication (Supporting Information, Figure S3). The indium tin oxide (ITO)-coated glass wafer was selected for its electrical and optical properties. High electrical conductivity of ITO was used for trapping the particles conjugated with biological molecules. On the other hand, the high refractive index of ITO contributed to create wave-guided modes in the nanoarrays. In addition, its optical transparency aided optic-based detection. Before coating the resist, the wafer was washed with acetone and fully spin-dried. LOL-2000 was spin-coated on the wafer at 6500 rpm for 45 s, followed by being baked at 180 °C for 300 s. After cooling the wafer, 2% 950 PMMA A2 was spin-coated on the LOL-ITO-glass wafer at 500 rpm for 5 s followed by 3000 rpm for 45 s. The wafer was then placed on a hot plate at 180 °C for 80 s. Eventually the bilayer coating procedure made a total 240 nm thickness coating. The thickness was measured by an ellipsometer (Auto EL-2, Rudolph Research Analytical, Hackettstown, NJ, U.S.A.). The coated wafer was cut into 37.5 × 25 mm chips. The chip was patterned using a scanning electron microscope (SEM) equipped with a nanometer pattern generation system (NPGS, FI 430 NanoSEM electron beam lithography system, FEI, Hillsboro, OR, U.S.A.) at 30 KeV, 24 pA beam current, and 1.2 spot size. The chip was then developed using 1:3 MIBK/IPA for 90 S, followed by being rinsed with IPA for 60 s.[46] To fully eliminate any LOL-2000 residue that remained on the ITO surface, additional developing was performed by using 1:5:5 CD-26/H_2O/IPA for 15 s. The chip was rinsed with DI water and dried.

Single Photon Counting Detection System. Supporting Information, Figure S4 shows the schematic of homemade epi-fluorescent single photon counting detection system. A particle trapped in the well was detected with a 100×-infinity corrected objective lens. A 532 nm CW laser was used to excite fluorescent probes of the immunocomplex. A 632 nm laser was used to image the fluorescent particles trapped into the wells. To guide the 532 or 632 nm laser to the nanoarray at sample stage and emitted light toward a SPAD or a CCD camera, the dual edges-beam splitter was located before a 75 mm focal length convex lens that was used as a tube lens for the infinity corrected lens. The light emitted from the immunocomplex or fluorescent particles through the objective, tube lens, and beam splitter was filtered to eliminate the background of 532 or 632 nm band and simultaneously transmit all other wavebands by using 532 nm long pass filter, 532 nm notch filter, and 633 nm notch filter. The detection sites were confirmed with the 20× or 10× eyepieces. The photons of light emitted from the immunocomplex were then collected by the SPAD which generated a pulse per a photon. The pulses were counted by using an oscilloscope (WavePro 7000; Lecroy, Chestnut Ridge, NY) connected to the SPAD.

Conflict of Interest: The authors declare no competing financial interest.

Acknowledgment. The authors thank the Northern California Nanotechnology Center at the University of California—Davis for the facilities used in the fabrication of nanoarrays and Professor T. Young for permission to use his zeta potential analyzer. We thank J. Nellis for his help in constructing the single photon counting detection system. The project described was supported by Award No. P42ES004699 from the National Institute of Environmental Health Sciences. The content is solely the responsibility of the authors and does not necessarily represent the official views of the National Institute of Environmental Health Sciences or the National Institutes of Health. This work was also supported by Grant 200911634 from NIAID, NIH. Additional support was provided by the National Research Initiative of the USDA Cooperative State Research, Education and Extension Service, Grant No. 2009-35603-05070.

Supporting Information Available: Figures S1−4 and Tables S1−3. This material is available free of charge *via* the Internet at http://pubs.acs.org.

REFERENCES AND NOTES

1. Peeters, J. K.; Spek, P. J. V. d. Growing Applications and Advancements in Microarray Technology and Analysis Tools. *Cell Biochem. Biophys.* **2005**, *43*, 149–166.
2. Chan, S. M.; Ermann, J.; Su, L.; Fathman, G.; Utz, P. J. Protein Microarrays for Multiplex Analysis of Signal Transduction Pathways. *Nat. Med.* **2004**, *10*, 1390–1396.
3. Lynch, M.; Mosher, C.; Huff, J.; Nettikadan, S.; Johnson, J.; Henderson, E. Functional Protein Nanoarrays for Biomarker Profiling. *Proteomics* **2004**, *4*, 1695–1702.
4. Lee, M.; Kang, D.-K.; Yang, H.-K.; Park, K.-H.; Choe, S. Y.; Kang, C.; Chang, S.-I.; Han, M. H.; Kang, I.-C. Protein Nanoarray on Prolinker Surface Constructed By Atomic Force Microscopy Dip-Pen Nanolithography for Analysis of Protein Interaction. *Proteomics* **2006**, *6*, 1094–1103.
5. Sinensky, A. K.; Belcher, A. M. Label-Free and High-Resolution Protein/DNA Nanoarray Analysis Using Kelvin Probe Force Microscopy. *Nat. Nanotechnol.* **2007**, *2*, 653–659.
6. Kang, S. H.; Kim, Y. J.; Yeung, E. S. Detection of Single-Molecule DNA Hybridization by Using Dual-Color Total Internal Reflection Fluorescence Microscopy. *Anal. Bioanal. Chem.* **2007**, *387*, 2663–2671.
7. Li, H.; Wang, J.; Pan, Z.; Cui, L.; Xu, L.; Wang, R.; Song, Y.; Jiang, L. Amplifying Fluorescence Sensing Based on Inverse Opal Photonic Crystal toward Trace TNT Detection. *J. Mater. Chem.* **2011**, *21*, 1730–1735.
8. Huang, C. S.; George, S.; Lu, M.; Chaudhery, V.; Tan, R. M.; Zangar, R. C.; Cunningham, B. T. Application of Photonic Crystal Enhanced Fluorescence to Cancer Biomarker Microarrays. *Anal. Chem.* **2011**, *83*, 1425–1430.
9. Block, I. D.; Mathias, P. C.; Ganesh, N.; Jones, S. I.; Dorvel, B. R.; Vikra, C.; Vodkin, L. O.; Bashir, R.; Cunningham, B. T. A Detection Instrument for Enhanced-Fluorescence and Label-Free Imaging on Photonic Crystal Surfaces. *Opt. Express.* **2009**, *17*, 13222–13235.
10. Zhao, Y.; Zhao, X.; Sun, C.; Li, J.; Zhu, R.; Gu, Z. Encoded Silica Colloidal Crystal Beads as Supports for Potential Multiplex Immunoassay. *Anal. Chem.* **2008**, *80*, 1598–1605.
11. Zhang, Y.; Wang, J.; Huang, Y.; Song, Y.; Jiang, L. Fabrication of Functional Colloidal Photonic Crystals Based on Well-Designed Latex Particles. *J. Mater. Chem.* **2011**, *21*, 14113–14126.
12. Li, H.; Wang, J. X.; Liu, F.; Song, Y. L.; Wang, R. M. Fluorescence Enhancement by Heterostructure Colloidal Photonic Crystals with Dual Stopbands. *J. Colloid Interface Sci.* **2011**, *356*, 63–68.
13. Shen, W. Z.; Li, M. Z.; Xu, L. A.; Wang, S. T.; Jiang, L.; Song, Y. L.; Zhu, D. B. Highly Effective Protein Detection for Avidin-Biotin System Based on Colloidal Photonic Crystals Enhanced Fluoroimmunoassay. *Biosens. Bioelectron.* **2011**, *26*, 2165–2170.
14. Zlatanovic, S.; Mirkarimi, L. W.; Sigalas, M. M.; Bynum, M. A.; Chow, E.; Robotti, K. M.; Burr, G. W.; Esener, S.; Grot, A. Photonic Crystal Microcavity Sensor for Ultracompact Monitoring of Reaction Kinetics and Protein Concentration. *Sens. Actuators, B* **2009**, *141*, 13–19.
15. El Beheiry, M.; Liu, V.; Fan, S. H.; Levi, O. Sensitivity Enhancement in Photonic Crystal Slab Biosensors. *Opt. Express.* **2010**, *18*, 22702–22714.
16. Chaudhery, V.; Huang, C.-S.; Pokhriyal, A.; Polans, J.; Cunningham, B. T. Spatially Selective Photonic Crystal Enhanced Fluorescnece and Application to Background Reduction for Biomolecule Detection Assays. *Opt. Express.* **2011**, *9*, 1–17.
17. Haukanes, B. I.; Kvam, C. Application of Magnetic Beads in Bioassays. *Biotechnology* **1993**, *11*, 60–63.
18. Morgan, E.; Varro, R.; Sepulveda, H.; Ember, J. A. Cytometric Bead Array: A Multiplexed Assay Platform with Applications in Various Areas of Biology. *Clin. Immunol.* **2004**, *110*, 252–266.
19. Wilson, R.; Cossins, A. R.; Spiller, D. G. Encoded Microcarriers for High-Throughput Multiplexed Detection. *Angew. Chem., Int. Ed.* **2006**, *45*, 6104–6117.
20. Kellar, K. L.; Kalwar, R. R.; Dubois, K. A.; Crouse, D.; Chafin, W. D.; Kane, B.-E. Multiplexed Fluorescent Bead-Based Immunoassays for Quantitation of Human Cytokines in Serum and Culture Supernatants. *Cytometry* **2001**, *45*, 27–36.
21. Krishhan, V. V.; Khan, I. H.; Luciw, P. A. Multiplexed Microbead Immunoassays by Flow Cytometry for Molecular Profiling: Basic Concepts and Proteomics Applications. *Crit. Rev. Biotechnol.* **2009**, *29*, 29–43.
22. Jager, W. d.; Rijkers, G. T. Solid-Phase and Bead-Based Cytokine Immunoassay: A Comparison. *Methods* **2006**, *38*, 294–303.
23. Han, J.-H.; Lakshmana, S.; Kim, H.-J.; Hass, E. A.; Gee, S.; Hammock, B. D.; Kennedy, I. M. High Performance Electrophoresis System for Site-Specific Entrapment of Nanoparticles in a Nanoarray. *Proc. SPIE* **2010**, 75740L.
24. Hessel, A.; Oliner, A. A. A New Theory of Woods Anomalies on Optical Gratings. *Appl. Opt.* **1965**, *4*, 1275–&.
25. Lam, C. C.; Leung, P. T.; Young, K. Explicit Asymptotic Formulas for the Positions, Widths, And Strengths of Resonances in Mie Scattering. *J. Opt. Soc. Am. B* **1992**, *9*, 1585–1592.
26. Rosenblatt, D.; Sharon, A.; Friesem, A. A. Resonant Grating Waveguide Structures. *IEEE J. Quantum Electron.* **1997**, *33*, 2038–2059.
27. Rissin, D. M.; Kan, C. W.; Campbell, T. G.; Howes, S. C.; Fourniew, D. R.; Song, L.; Piech, T.; Patel, P. P.; Chang, L.; Rivnak, A. J.; Fereel, E. P.; Randall, J. D.; Provuncher, G. K.; Walt, D. R.; Duffy, D. C. Single-Molecule Enzyme-Linked Immunosorbent Assay Detects Serum Proteins at Subfemtomolar Concentrations. *Nat. Biotechnol.* **2010**, *28*, 595–599.
28. Wild, D., *The Immunoassay Handbook*, 3rd ed.; Elsevier: New York, NY, 2005.
29. Gohring, J. T.; Dale, P. S.; Fan, X. Detection of HER2 Breast Cancer Biomarker Using the Opto-Fluidic Ring Resonator Biosensor. *Sens. Actuators, B* **2010**, *146*, 226–230.
30. Ganesh, N.; Zhang, W.; Mathias, P. C.; Chow, E.; Soares, J. A. M. T.; Malyarchuk, V.; Smith, A. D.; Cunningham, B. T. Enhanced Fluorescence Emission from Quantum Dots on a Photonic Crystal Surface. *Nat. Nanotechnol.* **2007**, *2*, 515–520.
31. Goh, J. B.; Tam, P. L.; Loo, R. W.; Goh, M. C. A Quantitative Diffraction-Based Sandwich Immunoassay. *Anal. Biochem.* **2003**, *313*, 262–266.
32. Han, J.-H.; Kim, K.-S.; Yoon, J.-Y. The Enhanced Diffusional Mixing for Latex Immunoagglutination Assay in a Microfluidic Device. *Anal. Chim. Acta* **2007**, *584*, 252–259.
33. Dee, K. C.; Puleo, D. A.; Bizios, R. *An Introduction to Tissue-Biomaterial Interactions*; John Wiley & Sons, Inc.: Hoboken, NJ, 2002.
34. Rucker, V. C.; Havenstrite, K. L.; Simmons, B. A.; Sickafoose, S. M.; Herr, A. E.; Shediac, R. Functional Antibody Immobilization on 3-Dimensional Polymeric Surfaces Generated by Reactive Ion Etching. *Langmuir* **2005**, *21*, 7621–7625.
35. Liu, Y.; Hu, W.; Lu, Z.; Li, C. M. Photografted Poly(methyl methacrylate)-Based High Performance Protein Microarrays for Hepatitis B Virus Biomarker Detection in Human Serum. *Med. Chem. Commun.* **2010**, *1*, 132–135.
36. Kusnezow, W.; Syagailo, Y. V.; Ruffer, S.; Baudenstiel, N.; Gauer, C.; Hoheisel, J. D.; Wild, D.; Goychuk, I. Optimal Design of Microarray Immunoassays to Compensate for Kinetic Limitation. *Mol. Cell Proteomics* **2006**, *5*, 1681–1696.
37. Ekins, R. P.; Berger, H.; Chu, F. W.; Finckh, P.; Krause, F. Miniaturized Immunoassays: Ultrasensitive Multianalyte Immunoassays on a Chip. *Nanobiology* **1998**, *4*, 197–220.
38. Chang, L.; Rissin, D. M.; Fournier, D. R.; Piech, T.; Patel, P. P.; Wilson, D. H.; Duffy, D. C. Single Molecule Enzyme-Linked Immunosorbent assays: Theoretical Considerations. *J. Immunol. Methods* **2012**, *378*, 102–115.
39. Ghitescu, L.; Bendayan, M. Immunolabeling Efficiency of Protein A-Gold Complexes. *J. Histochem. Cytochem.* **1990**, *38*, 1523–1530.
40. Jiang, W.; Kim, B. Y. S.; Rutka, J. T.; Chan, W. C. W. Nanoparticle-Mediated Cellular Response Is Size-Dependent. *Nat. Nanotechnol.* **2008**, *3*, 145–150.

41. Sheehan, P. E.; Whitman, L. J. Detection Limits for Nanoscale Biosensors. *Nano Lett.* **2005**, *5*, 803–807.
42. Johnson, R. D.; Arnold, F. H. The Temkin Isotherm Describes Heterogeneous Protein Adsorption. *Biochim. Biophys. Acta* **1995**, *1247*, 293–297.
43. Wijaya, I. P. M.; Nie, T. J.; Gandhi, S.; Boro, R.; Palaniappan, A.; Hau, G. W.; Rodriguez, I.; Suri, C. R.; Mhaisalkar, S. G. Femtomolar Detection of 2,4-Dichlorophenoxyacetic Acid Herbicides *via* Competitive Immunoassays Using Microfluidic Based Carbon Nanotube Liquid Gated Transistor. *Lab Chip* **2010**, *10*, 634–638.
44. Nam, J.-M.; Thaxton, C. S.; Mirkin, C. A. Nanoparticle-Based Bio−Bar Codes for the Ultrasensitive Detection of Proteins. *Science* **2003**, *301*, 1884–1886.
45. Munge, B. S.; Coffey, A. L.; Doucette, J. M.; Somba, B. K.; Malhotra, R.; Patel, V.; Gutkind, J. S.; Rusling, J. F. Nanostructured Immunosensor for Attomolar Detection of Caner Biomarker Interleukin-8 Using Massively Labeled Superparamagnetic Particles. *Angew. Chem.* **2011**, *123*, 8061–8064.
46. Tseng, A. A.; Chen, K.; Chen, C. D.; Ma, K. J. Electron Beam Lithography in Nanoscale Fabrication: Recent Development. *IEEE Trans. Electron. Packag. Manuf.* **2003**, *26*, 141–149.

SUPPORTING INFORMATION

for

Ultrasensitive immunoassays with a nanoparticle-based photonic crystal

Jin-Hee Han[1], L. Sudheendra[1], Hee-Joo Kim[2], Shirley J. Gee[2], Bruce D. Hammock[2], Ian M. Kennedy[1]

[1]Department of Mechanical and Aerospace Engineering

[2]Department of Entomology, University of California, Davis, California 95616, USA.

Correspondence should be addressed to I. M. K. (imkennedy@ucdavis.edu).

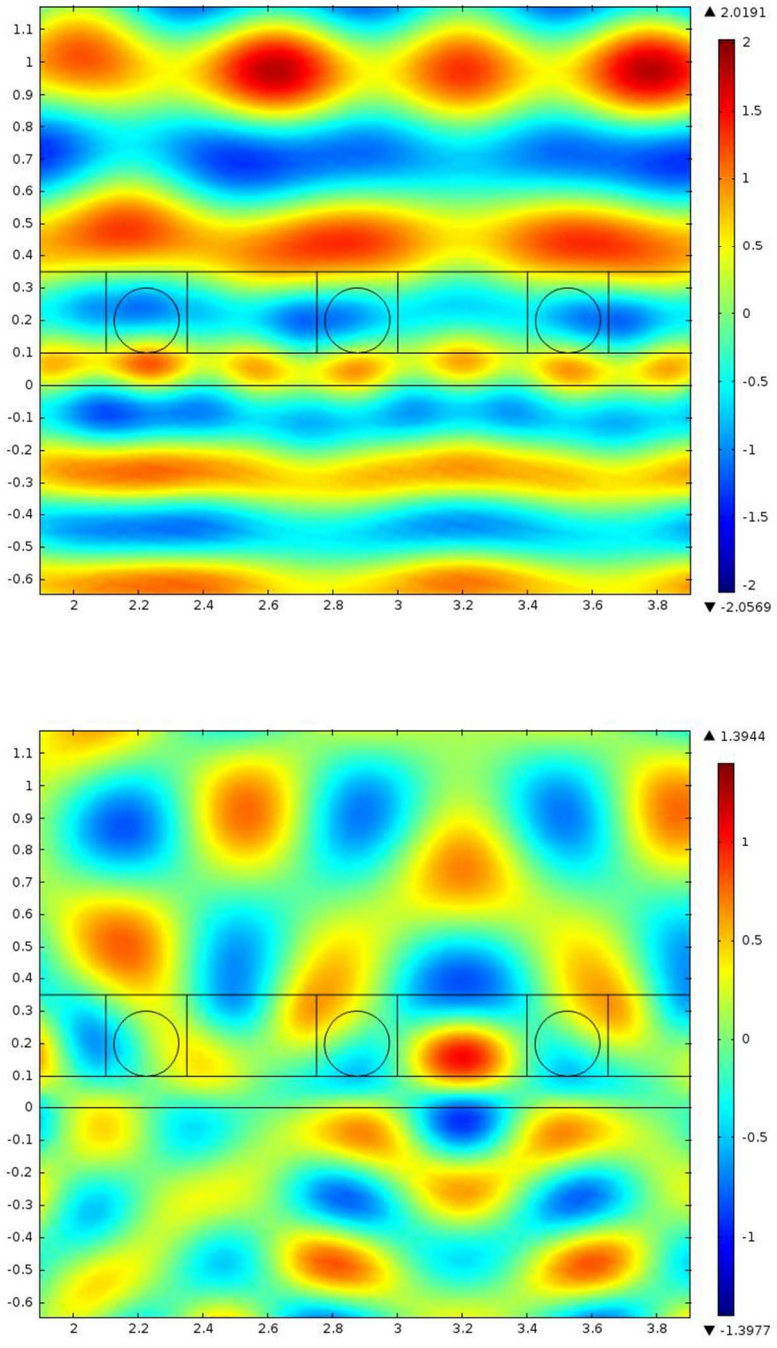

Supplemental Figure S1. Numerical modeling of the nanoarray with PC structure. (top) 200 nm-particles with 650 nm-periodicity for 532 nm-wavelength, (bottom) 555 nm-wavelength.

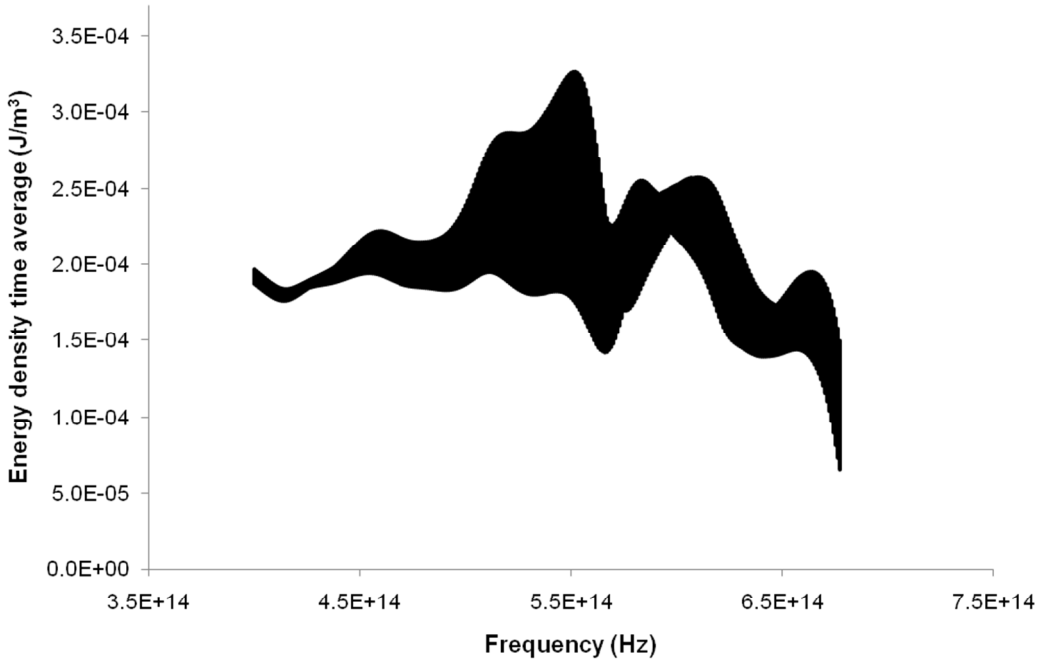

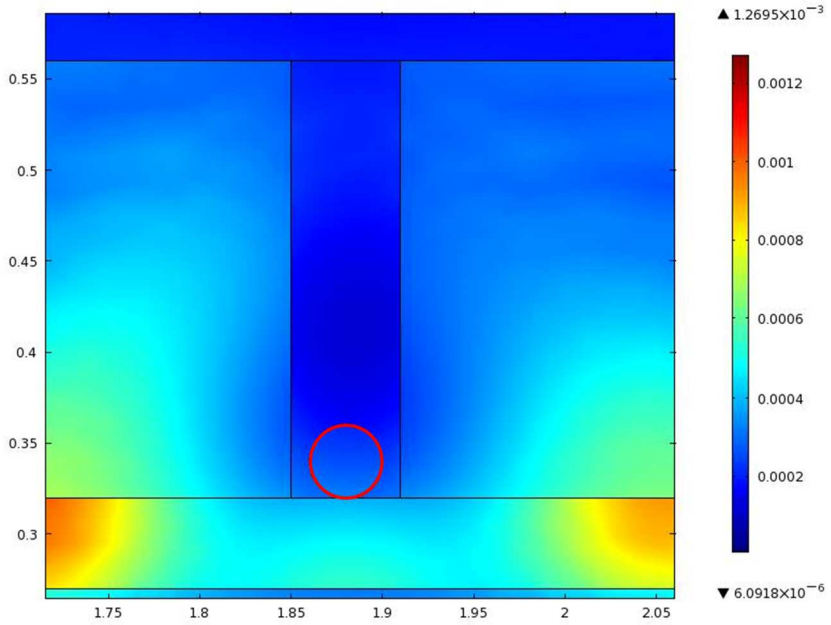

Supplemental Figure S2. Energy density time average as a function of frequency showing resonance. Data on the graph corresponds to the surface of the particles in wells (red circle).

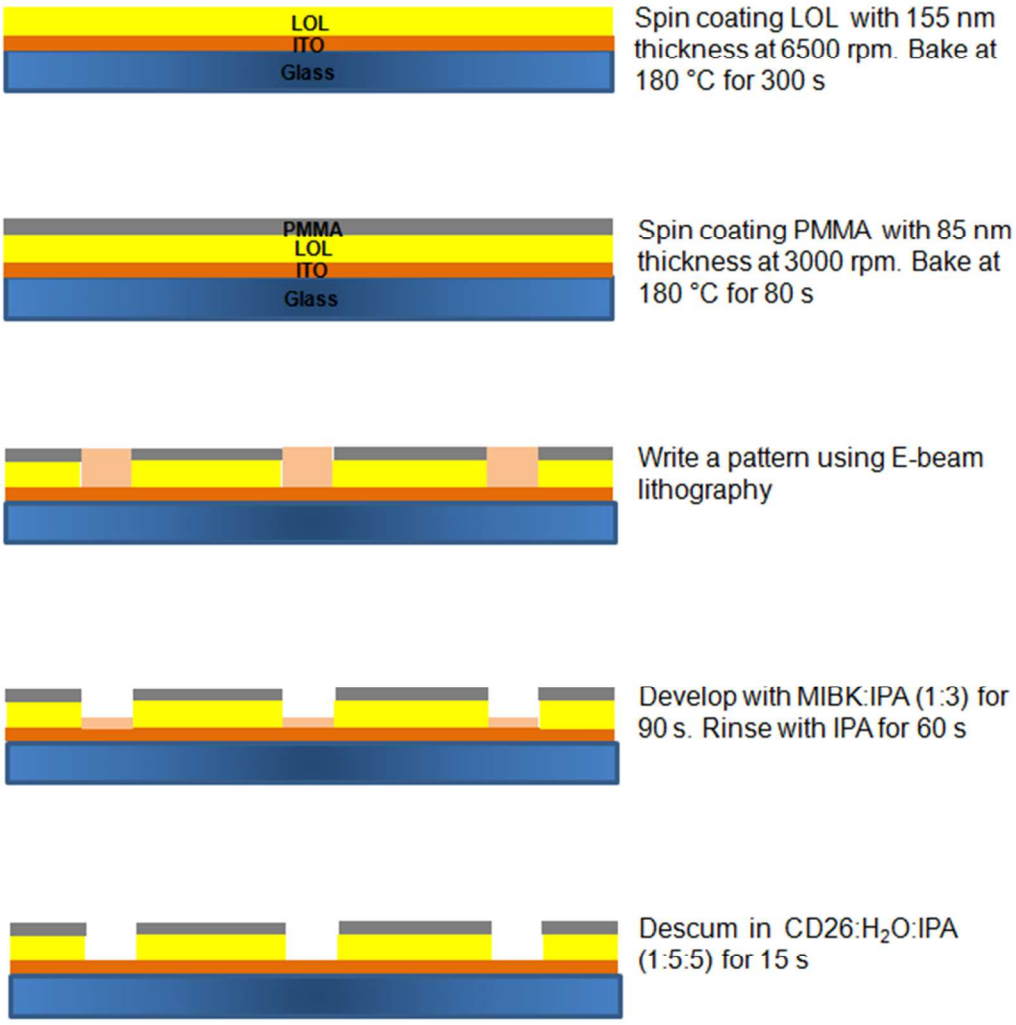

Supplemental Figure S3. Fabrication of nano- or micro- arrays/well.

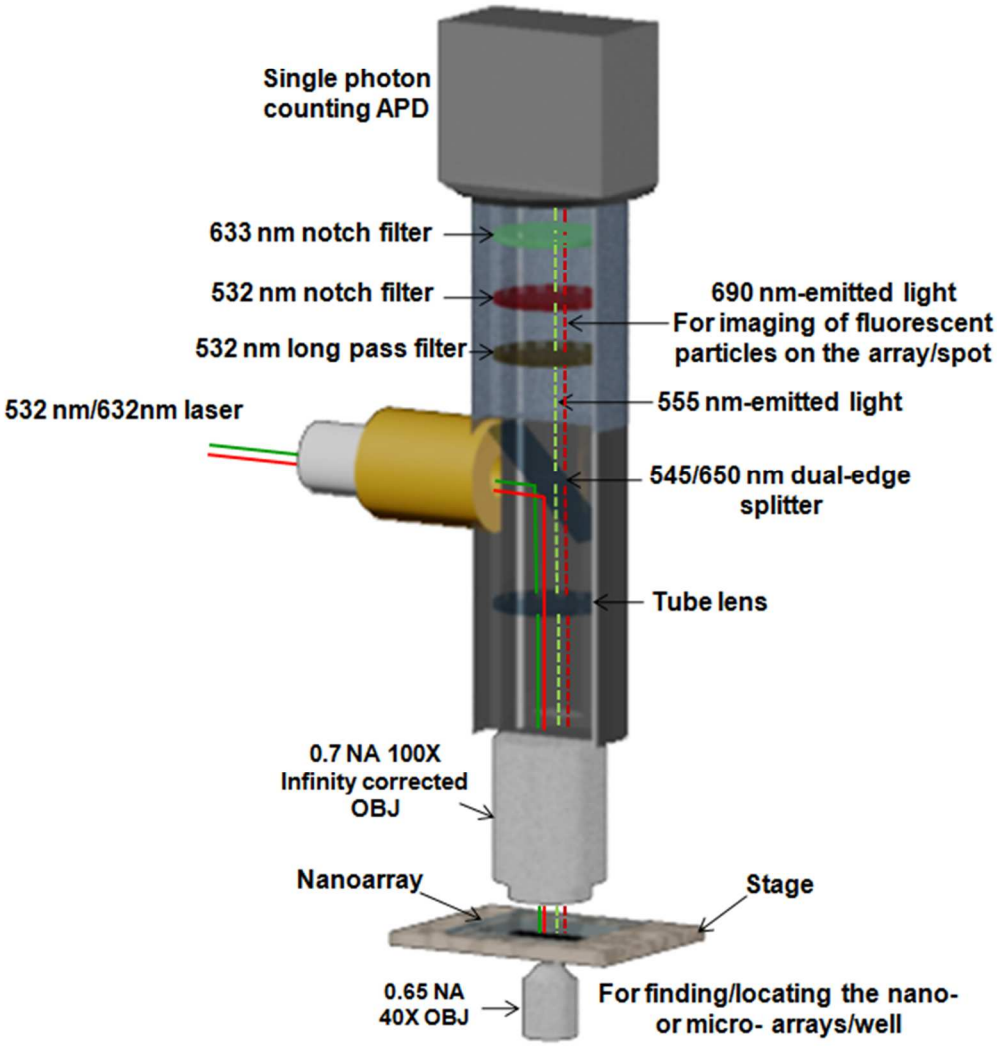

Supplemental Figure S4. The schematic of the single photon counting detection system.

Supplemental Table S1. Properties of materials used in the numerical model

	Refractive index	Relative permeability	Relative permittivity	Electrical conductivity (S/m)
PMMA	1.53	0.9	3.0	10^{-19}
Glass	1.50	1.0	4.8	10^{-14}
Polystyrene	1.55	0.9	2.5	10^{-16}
AIR	1.0	1	1	10^{-30}
ITO	2.0	1	3.6	4500

In refractive index of the PMMA, the averaged value of PMMA (1.48) and LOL (1.58) was used.

Supplemental Table S2. Fluorescent signals on a 40 nm-nanoarray with 650 nm-periodicity using two different refractive index materials-periodic structures

	Glycerine-PMMA	Water-PMMA	Air-PMMA
Signal (photons/second)	134±23	570±65	757±58

The concentration of the target analyte (rabbit-IgG): 10 μg/ml

Supplemental Table S3. The datum points used on the standard curve for quantifying rabbit IgG

Arrays/Spot	Fluorescent signal ± SD (photons/second)									
	1000 µg/ml	10 µg/ml	10 µg/ml	1 µg/ml	0.1 µg/ml	0.01 µg/ml	0.001 µg/ml	10^{-6} µg/ml	NC	NSB
5 µm	135±19	132±34	116±11	46±28	-	-	-	-	18±1	31±2
1 µm	201±20	278±0	246±31	107±0	64±20	61±5	43±1	-	16±5	18±2
200 nm	398±46	442±0	422±31	344±16	258±14	231±46	211±0	89±12	24±6	23±2
40 nm	761±57	762±0	775±58	663±4	404±0	365±36	204±6	43±3	17±3	31±2
BN	13±4									

SD: Standard deviation over three replicates, NC: Negative control, NSB: Non-specific binding, BN: Background noisy